ACSNANO

www.acsnano.org

ARTICLE

Controlling the Polarization State of Light with Plasmonic Metal Oxide Metasurface

Jongbum Kim,[†] Sajid Choudhury,[†] Clayton DeVault,[‡] Yang Zhao,[§] Alexander V. Kildishev,[†] Vladimir M. Shalaev,[†] Andrea Alù,[∥] and Alexandra Boltasseva*[,†]

[†]School of Electrical & Computer Engineering and Birck Nanotechnology Center and [‡]Deptartment of Physics and Astronomy and Birck Nanotechnology Center, Purdue University, West Lafayette, Indiana 47907, United States

[§]Materials Science and Engineering, Stanford University, Stanford, California 94305, United States

[∥]Department of Electrical and Computer Engineering, The University of Texas at Austin, 1 University Station C0803, Austin, Texas 78712, United States

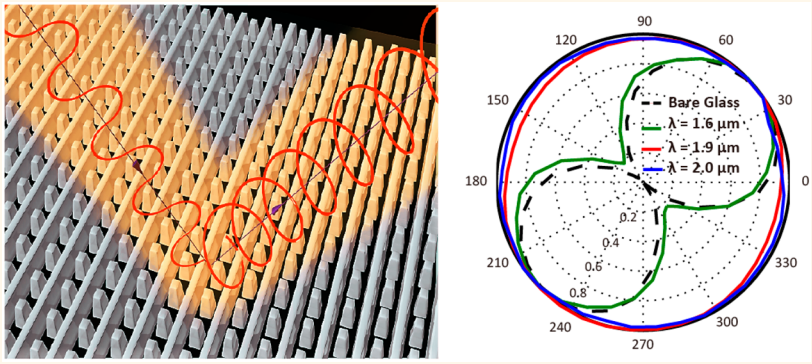

ABSTRACT: **Conventional plasmonic materials, namely, noble metals, hamper the realization of practical plasmonic devices due to their intrinsic limitations, such as lack of capabilities to tune in real-time their optical properties, failure to assimilate with CMOS standards, and severe degradation at increased temperatures. Transparent conducting oxide (TCO) is a promising alternative plasmonic material throughout the near- and mid-infrared wavelengths. In addition to compatibility with established silicon-based fabrication procedures, TCOs provide great flexibility in the design and optimization of plasmonic devices because their intrinsic optical properties can be tailored and dynamically tuned. In this work, we experimentally demonstrate metal oxide metasurfaces operating as quarter-waveplates (QWPs) over a broad near-infrared (NIR) range from 1.75 to 2.5 μm. We employ zinc oxide highly doped with gallium (Ga:ZnO) as the plasmonic constituent material of the metasurfaces and fabricate arrays of orthogonal nanorod pairs. Our Ga:ZnO metasurfaces provide a high degree of circular polarization across a broad range of two distinct optical bands in the NIR. Flexible broadband tunability of the QWP metasurfaces is achieved by the significant shifts of their optical bands and without any degradation in their performance after a post-annealing process up to 450 °C.**

KEYWORDS: *plasmonics, metal oxides, metasurface, surface plasmon resonance, quarter-waveplate, semiconductor*

Flat photonics is an emerging field in nano-optics that utilizes the concept of metasurfaces.[1−3] With the advent of metasurfaces, fabrication challenges associated with volumetric metamaterials can be easily overcome. Metasurfaces can push conventional optical components to the subwavelength scale, paving the way for ultracompact devices and on-chip optical processing. By altering the phase of the incoming light, metasurfaces have enabled many applications, such as 3D holograms,[4−7] flat lenses,[8−10] beam splitters,[11,12] and waveplates,[13−17] with a device thickness of only a fraction of the wavelength. The significant interest in advanced optical signaling and sensors[18,19] has led to the development of metasurfaces with quarter-waveplate (QWP) functionalities, converting linearly polarized light into circularly polarized light and *vice versa*. With noble metals, metasurfaces, which consist of arrays of orthogonally coupled nanoantennas[16,20,21] and V-shaped antennas,[13] have been used to demonstrate waveplate operation with deeply subwavelength profiles. In addition, metasurfaces have been placed on a reflective metal mirror to achieve high efficiency in the terahertz regime.[22,23] Furthermore, dielectric metasurfaces have been introduced to design QWP metasurfaces in the near-infrared (NIR) range.[24] Although these metasurfaces have achieved the desired

Received: June 14, 2016
Accepted: October 5, 2016
Published: October 5, 2016

DOI: 10.1021/acsnano.6b03937
ACS Nano 2016, 10, 9326−9333

function, they pose integration challenges, often exhibit considerable optical losses, and do not offer switchability/tunability of their optical properties. For practical applications, it is more desirable to fabricate these metasurfaces with a versatile, tunable, and CMOS-compatible material.

To date, there is a growing body of research on transparent conducting oxides (TCOs) as an alternative material platform for near- and mid-infrared plasmonics.[25−27] TCOs (*e.g.*, aluminum- or gallium-doped zinc oxide [Al:ZnO, Ga:ZnO], tin-doped indium oxide [ITO], indium-doped cadmium oxide [ICO]) are highly doped wide band gap semiconductors with a plasma frequency typically in the NIR range.[25,28,29] Advantages of TCOs over noble metals include compatibility with a conventional fabrication technique, chemical and mechanical stabilities, and low intrinsic optical losses due to the wide band gap and small Drude damping (γ).[28,30] TCOs provide the capability of tailoring the intrinsic plasma frequency over a wide range due to their nonstoichiometric properties.[25] The surface plasmon resonance in various types of TCO nanostructures has been experimentally demonstrated, which makes TCOs very promising alternatives to noble metals for applications in the IR spectral range.[31−34] However, despite investigations of various TCO nanostructure geometries, little attention has been paid to control of the polarization state of light using nanoscale TCO resonators.

In this work, we experimentally realize a TCO metasurface to control the polarization of light in the reflection mode, spanning a broad bandwidth in the NIR regime. The metasurface is realized interleaving two orthogonal patterned nanorod arrays made of Ga:ZnO. A similar design has been proposed and experimentally demonstrated with silver (Ag) as the plasmonic component to operate in the visible range.[20] To achieve the quarter-waveplate functionality, in this design, the two perpendicular nanorods resonate at approximately equal amplitudes and a phase difference of $\pi/2$ in orthogonal polarizations. Compared to noble metals, TCOs have a relatively less dispersive dielectric function, which offers a broader bandwidth of operation for TCO-based metasurfaces in the NIR range. Additionally, through a post-annealing process, we can control the carrier density in TCO, thus further tuning the efficiency and bandwidth of the realized metasurfaces. This method relies on controlling the oxygen vacancy formation to adjust the free electron concentration, and it has been demonstrated to adjust the resonance frequencies of simple TCO geometries such as nanodisks and nanorods.[32,35,36] Furthermore, we show that changing the angle of incidence our TCO metasurfaces can provide QWP functionality in two distinct NIR optical bands.

RESULTS AND DISCUSSION

Two orthogonal nanorods provide the array element for our metasurface, as shown in Figure 1a. Each nanorod acts as a local antenna when excited at the resonance by the incident light with a particular direction, amplitude, and phase. Since the phase of the scattered fields sharply varies with the frequency around the nanorod resonance, it is possible to tailor the phase shift between the scattered waves of two orthogonal nanorods by slightly changing their relative lengths. In our design, we chose the lengths of orthogonal nanorod pairs such that linearly polarized light incident on our metasurface at an angle θ is converted to circularly polarized light over a particular spectral range. As illustrated in Figure 1b, the polarization angle ϕ is defined in the plane of the metasurface. To ensure a broad bandwidth, the horizontal rods are joined into a continuous strip and vertical rods are reduced to squares, as shown in Figure 1a,b. We obtained the optimized dimension of each Ga:ZnO rod through an analytical model provided in the recent work on metasurfaces based on orthogonally aligned silver nanorods.[7,21,37] The analytical model ensures that the reflection matrix of such a metasurface can be described as[14,20]

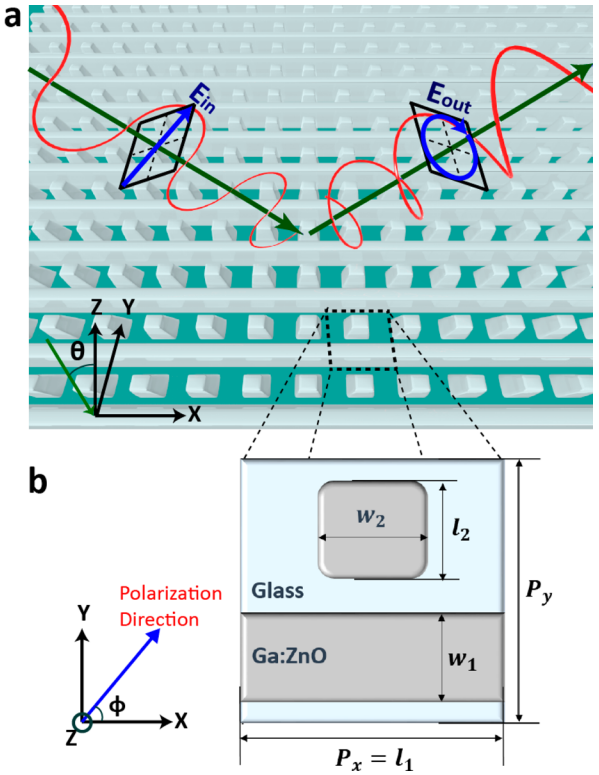

Figure 1. (a) Schematic view of an array of metal oxide nanostructures forming a metasurface. θ is the angle of incidence. The metasurface serves as a quarter-waveplate by converting a linearly polarized light to circularly polarized light in reflection mode. (b) Unit cells of plasmonic metasurfaces and the corresponding geometrical parameters. ϕ is the direction of polarization of incident wave. l_m and w_m (m = 1, 2) are the length and width of two nanorods, respectively. P_x and P_y is the periodicity in x- and y-directions. P_y is fixed at 750 nm, but P_x is varied from 550 to 750 nm to change the coupling efficiency of the two orthogonal nanorods.

$$R = \begin{pmatrix} R_{xx} & 0 \\ 0 & R_{yy} \end{pmatrix} = \begin{pmatrix} -\frac{j\mu_0 \pi f c \cos\theta}{P_x P_y} \frac{a_{xx}}{1 - C_{\mathrm{int},xx} a_{xx}} & 0 \\ 0 & -\frac{j\mu_0 \pi f c \cos\theta}{P_x P_y} \frac{a_{yy}}{1 - C_{\mathrm{int},yy} a_{yy}} \end{pmatrix} \quad (1)$$

DOI: 10.1021/acsnano.6b03937
ACS Nano 2016, 10, 9326−9333

where f is the frequency of operation, c is the speed of light in vacuum, μ_0 is the permeability of free space, and C_{int} is the interaction dyadic.[37,38] From the three-axial ellipsoid quasi-static polarizability with semiaxes $w/2$, $l/2$, and $t/2$, the polarizability tensor (a_{ii}, i = x,y,z) can be calculated as $a_{ii} = \frac{\pi}{2} wlt(\varepsilon_{Ga:ZnO} - \varepsilon_m)/[3\{\varepsilon_m + L_i(\varepsilon_{Ga:ZnO} - \varepsilon_m)\}]$, where L_i is the shape factor and ε_m is the permittivity of the surrounding medium of the nanorod. Considering the fabrication limitations, we optimize the metasurface with a constant thickness (t = 550 nm), width (w_1 = 250 nm and w_2 = 300 nm), and length of the horizontal nanorod (l_2 = 300 nm) but vary the length of the horizontal nanorod (l_1) from 550 to 750 nm with 100 nm increments to control the bandwidth of operation. As the length of the vertical nanorod is varied, the periodicity in the x-direction is also varied accordingly. TCO-based QWP metasurfaces require that the thickness (t = 550 nm) of the nanorods is 1 order of magnitude larger than that of a corresponding silver metasurface due to its low magnitude of real part of permittivity.

To fabricate the metasurface, we developed a dry-etching technique with bilayer resists—hydrogen silsesquioxane (HSQ) for the masking layer and poly(methyl methacrylate) (PMMA) for the sacrificial layer. As shown in the schematic of the fabrication flow (Figure 2a), a 550 nm thick Ga:ZnO film is deposited on a glass substrate by pulsed laser deposition (PVD Products, Inc.). On top of the deposited Ga:ZnO film, we spin-coat a 100 nm thick layer of PMMA at 4000 rpm followed by the sample prebake at 80 °C for 5 min. Once the PMMA layer is baked, we spin-coat a 500 nm thick layer of HSQ. The sample is prebaked again at 80 °C for 5 min. The nanoscale pattern of QWP is then exposed by electron beam lithography (Vistec VB6). An exposed sample is developed in 25% tetramethylammonium hydroxide (TMAH) for 1 min, dipped in DI water for 30 s to rinse off the TMAH, and then dried in gaseous nitrogen. The PMMA layer is etched by oxygen gas, and the TCO film is etched by chlorine gas with reactive ion etching (RIE). Ga:ZnO film is etched down 1.2 times faster than HSQ, hence a 500 nm thick nanorod can be patterned with 500 nm thick HSQ as the masking layer. When the design of the QWP metasurface is transferred to the Ga:ZnO layer, the sample is dipped into acetone to remove the PMMA layer with the remaining HSQ. The field emission scanning electron microscope (FESEM) images in Figure 2b,c provide a different view of the fabricated Ga:ZnO metasurface. The shape of the square particles becomes rounded during the etching process, but the size of structures is maintained as the original design.

To find the spectral range of QWP operation, it is necessary to characterize the resonance positions in two orthogonal polarizations because QWP functionality can be achieved from abrupt phase variations near the resonances that induce birefringence in anisotropic nanorod arrays. As already demonstrated in Ag-based waveplate metasurfaces, it is expected that the metasurface will serve as a waveplate in the spectral range between two resonances in orthogonal polarizations. The corresponding reflection spectra for the orthogonal linear polarizations (R_{xx} and R_{yy}) along the two rods with different periodicity in the x-direction are presented in Figure 3a. We notice that R_{xx} and R_{yy} have two pronounced resonant dips in the reflection spectra. To gain insight into the characteristics of the reflection resonances for both R_{xx} and R_{yy}, we validate the experimental spectra with numerical simulations using a commercially available software based on the finite element method (COMSOL Multiphysics), as shown in Figure 3b. We extracted the optical properties of Ga:ZnO by performing variable angle spectroscopic ellipsometry measurements (V-VASE, J.A. Woollam) on Ga:ZnO thin films; the extracted values are then used as the material properties in our simulation. The metasurface is simulated as a single unit cell with periodic boundary conditions. Ga:ZnO thin films are metallic for the wavelengths longer than 1.18 μm.[39] Overall, the resonance dips are weaker in the experiments than in the simulations due to inevitable fabrication imperfections, such as

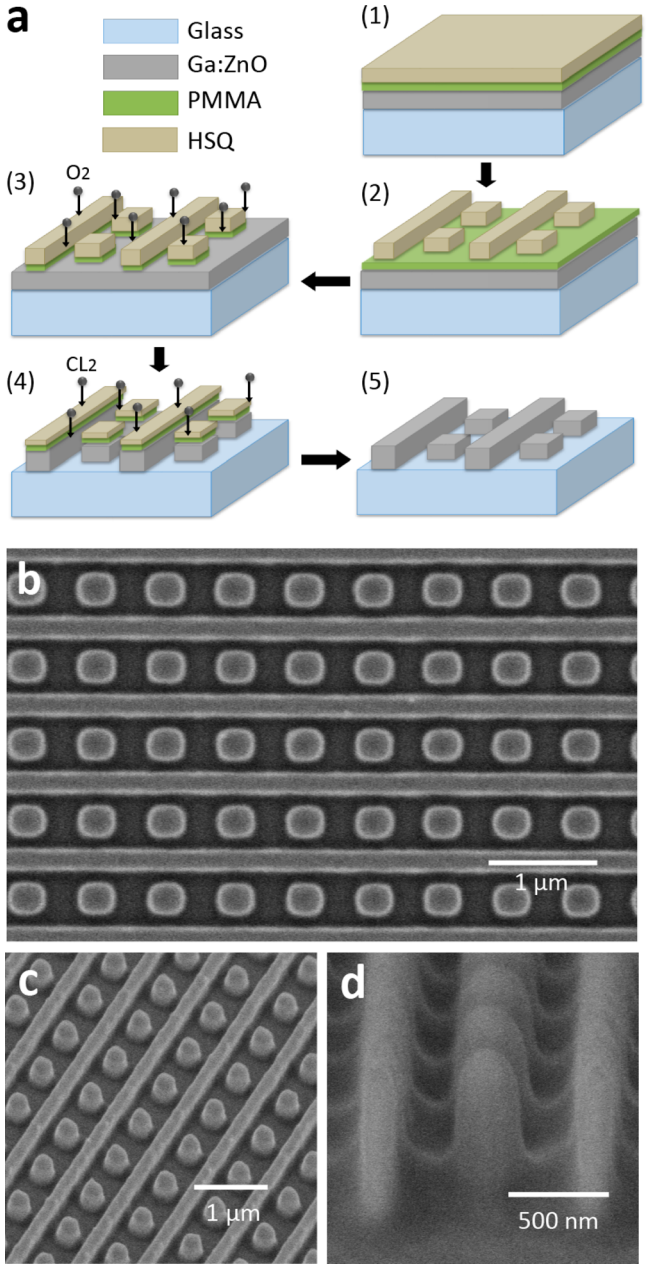

Figure 2. (a) Process flow for fabrication of Ga:ZnO metasurfaces using ion reactive etching with bilayer resist. (1) Spin-coating of PMMA and HSQ layer over Ga:ZnO film, (2) e-beam lithography of HSQ resist, (3) O_2 RIE etch of PMMA with HSQ as the etch mask, (4) CL_2 RIE etch of Ga:ZnO with HSQ and PMMA as the etch mask, and (5) removal of PMMA and HSQ etch mask with acetone. (b) Top view, (c) 30° tilted view, and (d) cross-sectional (75° tilted) view of the FESEM image of a fabricated Ga:ZnO metasurface.

DOI: 10.1021/acsnano.6b03937
ACS Nano 2016, 10, 9326−9333

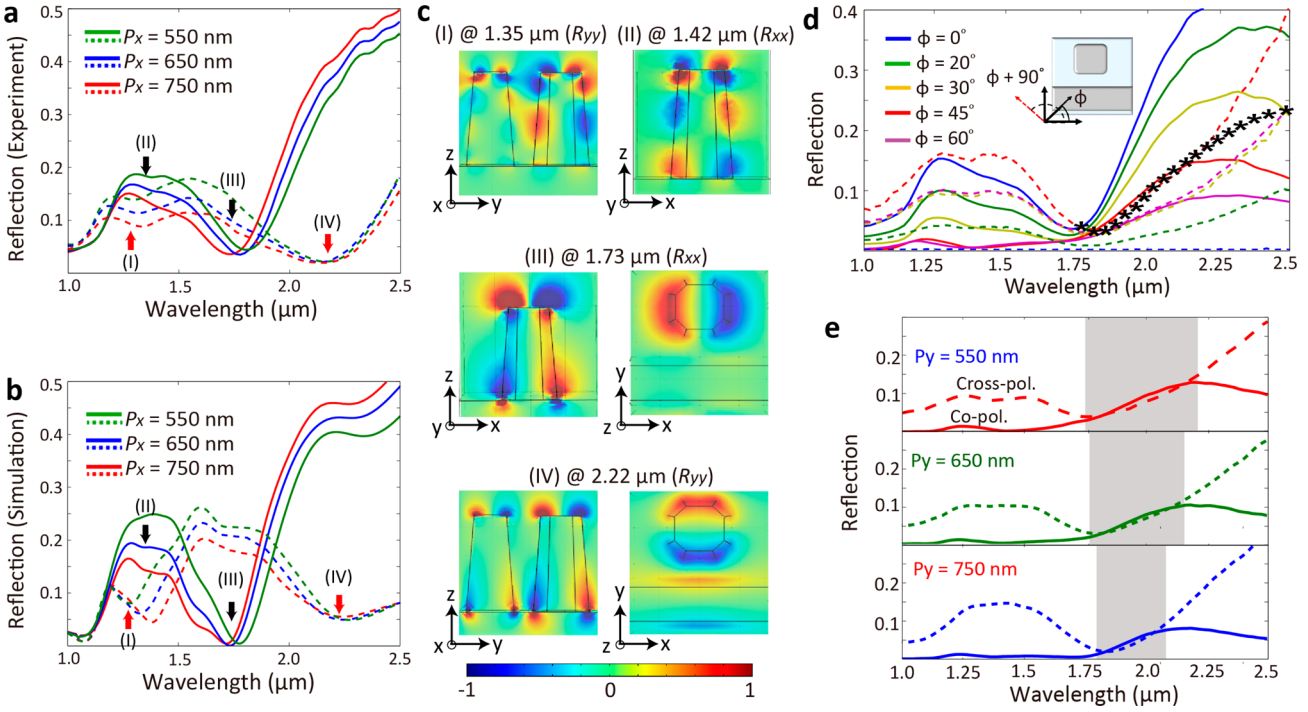

Figure 3. (a) Experiment and (b) simulation of reflection spectra of Ga:ZnO metasurfaces for orthogonal linear polarizations: R_{xx} (solid line) and R_{yy} (dashed line). (c) Cross-sectional, top-view, near-field distributions of Ga:ZnO metasurface (P_x = 750 nm) at the wavelengths of interests: (I), (II), (III), and (IV) in reflection spectra (a) and (b). The intensity of the electric field is normalized to the electric field of the incident wave. (d) Experimental co- and cross-polarized reflection spectra of metal oxide metasurface with different angles (ϕ) of polarization direction. The black marker indicates the wavelength where the intensity ratio is 1. Inset: Schematic image of unit cell of metasurface; ϕ is the polarization direction of incidence and ϕ + 90° is the cross-polarization in the reference to the polarization of incidence. (e) Experimental co- and cross-polarized reflection spectra of metal oxide metasurface with different P_x when the incident light is polarized to 45°. Highlighted area is the wavelength range where the intensity ratio of co- and cross-polarization is 1 ± 0.1.

the rounded shape and roughness of the sidewall. In addition, the optical properties of patterned TCOs change when compared to the properties of thin continuous films because nanofabrications introduce surface traps/states that change the carrier concentration.[34] We first explore the resonances dips in *y*-polarization by mapping the near-field distribution at the wavelengths of 1.35 μm (shown in Figure 3c(I)) and 2.22 μm (Figure 3c(IV)), where the strong dips are observed. The cross-sectional map of the electrical field's *z*-component (E_z) at the resonance in Figure 3c(I) shows that the fields are mostly enhanced between the nanorod and particles. Considering the permittivity of Ga:ZnO and the periodic arrangement of the metasurface, we can assume that the metasurface acts as a periodic geometrical grating; therefore, the absorption is enhanced at the resonance shown in Figure 3c(I). This feature is quite similar to the strong absorption of ITO nanorod arrays, which was attributed to the guided modes of surface plasmon of periodic arrays of nanostructures.[27,40] The field profile at the wavelength of 2.22 μm implies a localized surface plasmon resonance (LSPR) of the square particle in the direction of *y*-polarization. Two resonances in R_{xx} labeled (II) and (III) at 1.42 and 1.73 μm also support different modes of resonances, as shown in near-field distributions in Figure 3c.

The depolarization of light from anisotropic nanostructures is strongly dependent on the angle of polarization direction (ϕ) when the incident light is linearly polarized. As shown in the inset of Figure 3d, the depolarization of reflected light from the metasurface can be detected by polarization-selective measurements to probe the in- and out-of-plane polarization component of the scattered light from the metasurface. From the cross-polarized reflection measurement with different angle (ϕ) of polarization direction (Figure 3d), we see that the intensity of cross-polarized light in reference to the polarization direction of the incident wave reaches the maximum when the incident light is polarized at 45° with respect to the *x*-axis. The reflection data are measured from the design with P_x = 750 nm. The black marker shows the wavelength where the intensity ratio of the co- and cross-polarization component is exactly 1 with different angle (ϕ) of polarization direction, indicating that the metasurface can function as a QWP in this spectral range. Due to the relatively small dispersion of metal oxides, we can achieve the QWP functionality in a broad range of wavelengths with one angle of polarization direction when allowing 10% margin in the degree of polarization. As shown in Figure 3e, when the incident light is polarized to 45°, in the wavelength range highlighted by the gray area in the plot, the intensity ratio of the co- and cross-polarization component is 1 ± 0.1 and the metasurface can serve as QWP in the highlighted range. By increasing the periodicity of the *x*-direction (P_x), the bandwidth of the QWP operation becomes broader because the resonance in polarization of the *x*-direction is becoming red-shifted.

In addition to spectrum measurements, in order to demonstrate the operation of a TCO metasurface as QWP, we measured the phase difference (Δ) of the reflected light using spectroscopic ellipsometry to confirm the functionality. Spectroscopic ellipsometry measurement collects the phase difference (Δ) and the amplitude (Ψ) between two orthogonal polarization states. As described in eq 2, we can extract Δ of

DOI: 10.1021/acsnano.6b03937
ACS Nano 2016, 10, 9326−9333

two orthogonal polarizations (x- and y-component) from the ellipsometry measurement

$$\varphi = \frac{R_y}{R_x} = \tan(\psi)e^{i\Delta} \quad (2)$$

where R_x and R_y are the reflection of x- and y-polarization states and φ is the ellipsometry parameter. Figure 4a shows the

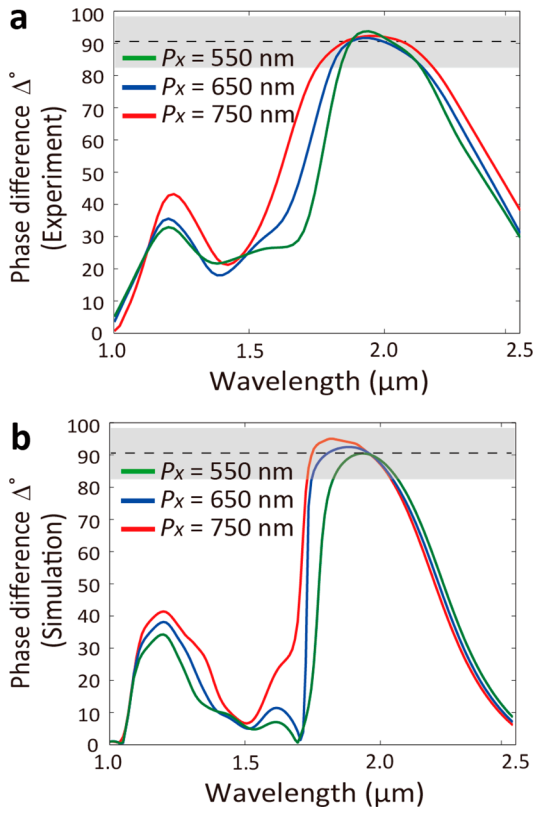

Figure 4. (a) Experimental and (b) simulated phase difference Δ of reflected light between two orthogonal polarizations (x and y) for 18° oblique incident light. The periodicity of the unit cell in y-direction is varied from 550 to 750 nm. The incident light is polarized to 45° with respect to the x-axis.

measured Δ of our metasurface at an angle of incidence θ = 18°. As expected from the reflection measurement, the TCO metasurface provides a wide range of quarter-waveplate functionality; for the case where P_x = 750 nm, the bandwidth is around 450 nm from λ = 1.75 μm to λ = 2.20 μm. To verify the measurement, the phase shift is calculated as the difference of phase angle for two orthogonal polarizations, as shown in Figure 4b. To avoid computational complexity, our simplified simulation model does not take into account scattering effects from the roughness of the sidewalls but only provides a very basic understanding of the operation of the quarter-waveplate. Thus, some discrepancies with the simulations and experiment is observed, but our ellipsometry results overall match well with our numerical simulations on the bandwidth variation with regards to the periodicity.

Consistent with the spectral range between two resonances corresponding to the excitation of the LSPR in two orthogonal polarizations, it is interesting to observe the phase variation between resonance (I) and (II) associated with the non-localized surface plasmon. By properly adjusting the size of each nanorod for detuning resonances, we are able to realize a 90° phase difference between the two resonances. Another method to control the phase difference is to change the angle of incident light. As presented in Figure 5a, the spectral range is

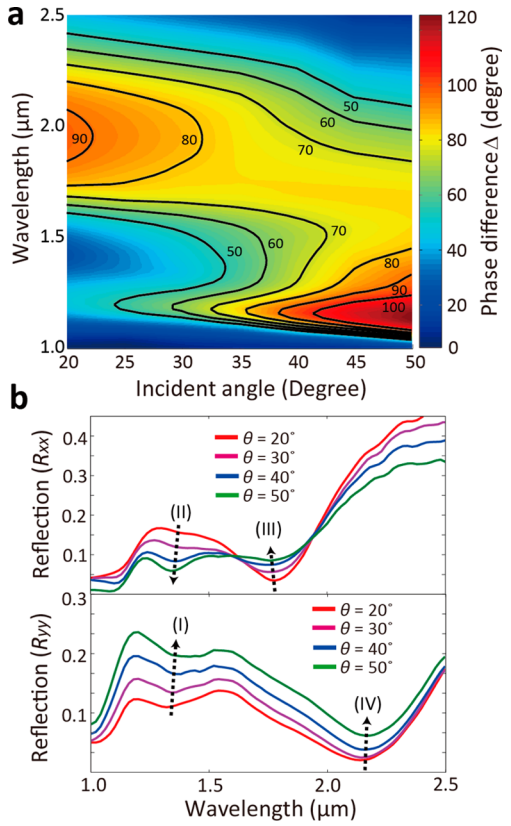

Figure 5. (a) Experimental phase difference Δ of the Ga:ZnO metasurface as a function of angle of incidence in the spectral range between 1 and 2 μm. The incident light is polarized to 45° with respect to the x-axis. Solid lines show corresponding phase differences with respect to different wavelengths and angles of incidence. (b) Reflection in x- and y-polarization (R_{xx} and R_{yy}) at various angles of incidence.

varied by changing the incidence angle. With increasing angle of incidence, the phase difference between the two LSPR resonances (III) and (IV) is reduced, whereas the phase difference between the resonance (I) and (II) is increased, as shown in Figure 5b. At an oblique angle of incidence, incoming light with polarization ϕ = 45° can be decomposed into x- and y-components with transverse magnetic (TM and TE) waves, respectively. For the TE case (R_{yy}), as the incidence angle increases gradually, a slight red shift of the reflection dip can be observed, with an increased reflectance over the entire visible region. In contrast to the behavior of the TE mode, the TM case (R_{xx}) drives a blue shift of the two resonances (I) and (IV); additionally, we see a strong absorption of the resonance associated with the nonlocalized plasmon mode (I) for the increasing angles of incidence.[41] Due to the opposite direction of resonance shifts with different polarizations, the two resonances (I) and (II) are getting closer so that the phase difference eventually reaches Δ = 90° at the angle of incidence of θ = 35°, whereas the phase difference between the two resonances (III) and (IV) are becoming smaller due to the increment of separation. Therefore, the TCO metasurface can span two spectral ranges in the NIR by controlling the incident

DOI: 10.1021/acsnano.6b03937
ACS Nano 2016, 10, 9326−9333

angle. However, it only covers a very narrow range of wavelengths between resonances (I) and (II).

To demonstrate our metasurface functionality as a waveplate, we measure the degree of circular polarization at λ = 1.9 and 2 μm by rotating a linear polarizer in front of a detector and measuring the reflected power, as depicted in Figure 6a. We

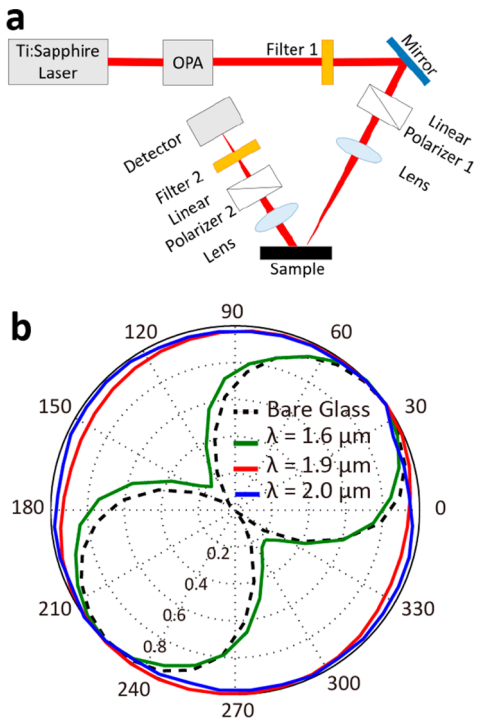

Figure 6. (a) Schematic of the optical setup to characterize the degree of circular polarization. Laser light is generated using an amplified Ti:sapphire femtosecond laser in combination with an optical parametric amplifier for infrared generation. Filters 1 and 2 are infrared long-pass and band-pass filters, respectively; filter 2's central wavelength was selected at 1.6, 1.9, and 2.0 μm depending on the wavelength of operation. Linear polarizer 1 defines the polarization of incoming wave (ϕ = 45°), and linear polarizer 2 is rotated while collecting the reflected power from the metasurface. (b) State-of-polarization analysis for the reflected beam at λ = 1.6, 1.9, and 2.0 μm. The reflected beam from a bare glass is collected at λ = 1.9 μm.

generated the infrared light using an amplified Ti:sapphire femtosecond laser followed by an optical parametric amplifier which was tuned over the 1.6−2 μm spectral range. We chose P_x = 750 nm, which provides the broadest bandwidth. A 45° polarized plane wave (ϕ = 45°) illuminated the metasurface, the same angle of polarization of the reflected light from the bare glass. The angle of incidence is fixed to 18° to be consistent with the ellipsometry measurement. As shown in Figure 6b, in comparison to the phase difference at the wavelength of 1.6 μm, where the metasurfaces cannot serve as a QWP, a high degree of circular polarization close to unity can be maintained at the wavelengths of 1.9 and 2 μm. These results substantially confirm the waveplate functionality of our Ga:ZnO metasurface and demonstrate that our devices are able to achieve a high degree of circular polarization (~98%) in the reflection mode over a broad range in the NIR.

One efficient method to engineer the resonance frequency of metal-oxide-based resonators without changing the design of the metasurface is postgrowth annealing.[32,35] Thermal annealing can efficiently reduce the carrier density and thereby provide a means for controlling the optical properties of the TCO materials, albeit irreversibly. As shown in eq 1, the polarizability tensor is a function of the permittivity of the metallic component. Thus, the operational range of the Ga:ZnO metasurface can be readily tuned through postgrowth annealing. Figure 7a presents the optical properties of Ga:ZnO

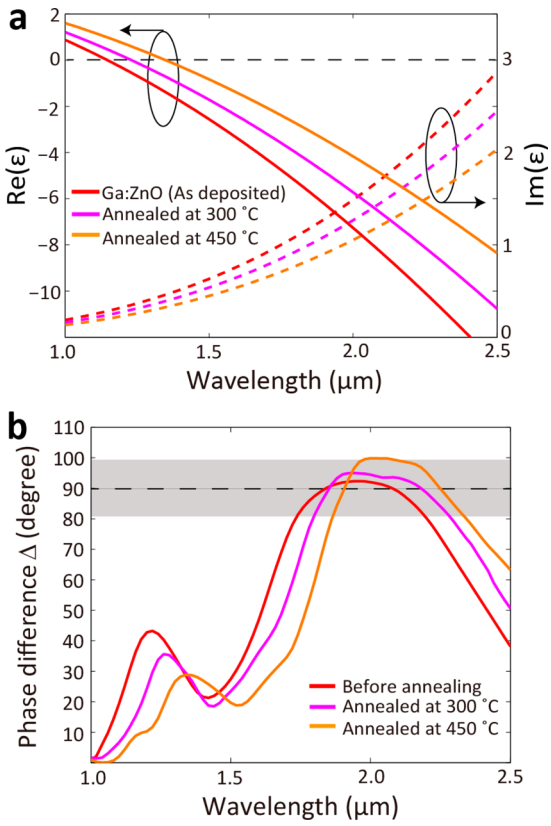

Figure 7. (a) Dielectric functions of Ga:ZnO thin film. Ga:ZnO films are annealed at 300 and 450 °C. (b) Phase difference Δ of reflected light from metasurface before and after annealing. Angle of incidence is 18°, and the incident light is polarized to 45° with respect to the *x*-axis. The periodicity of the unit cell in the *y*-direction is 750 nm.

films annealed at different temperatures in the nitrogen gas ambient for 1 h. These results show the tunability of optical properties of Ga:ZnO thin films through the annealing process. As a result of the decrease of intrinsic carrier density, we observe the shift of crossover wavelength with an increasing annealing temperature. This variation can be directly utilized to tune the functionality of a Ga:ZnO-based QWP metasurface, as shown in Figure 7b. We note that the operational range of the waveplate is shifted as much as the crossover wavelength of Ga:ZnO thin film is shifted by the post-annealing process.

CONCLUSION

We have experimentally demonstrated a plasmonic metasurface in the NIR using highly doped metal oxides that operates as a quarter-waveplate in the reflection mode. The broad bandwidth of QWP functionality is achieved due to slow dispersion of the dielectric function of Ga:ZnO. The experimental results agree well with our theoretical predictions and numerical simulations. Our TCO metasurface can be flexibly applied for a variety of spectral ranges by simply controlling the angle of incidence or

DOI: 10.1021/acsnano.6b03937
ACS Nano 2016, 10, 9326−9333

adjusting its intrinsic properties through a post-annealing process or other (electrical or optical) means, which is not achievable with noble-metal-based metasurfaces. In addition, conventional nanofabrication techniques are employed to realize TCO metasurfaces that offer easy integration with other nanophotonic devices that may require special polarization states. We believe that the broad-band performance, versatility, compactness, as well as integration advantages of the demonstrated waveplate can enable many practical applications of TCO metasurfaces in optical and nanophotonic technologies.

METHODS

Preparation of Ga:ZnO Thin Film. Ga:ZnO films were deposited by pulsed laser deposition (PVD Products, Inc.) using a KrF excimer laser (Lambda Physik GmbH) operating at a wavelength of 248 nm for source material ablation. The chosen ablation targets were 5 wt % (wt %) gallium-doped zinc oxide, which were purchased from the Kurt J. Lesker Corp. with purities of 99.99% or higher. The energy density of the laser beam at the target surface was maintained at 1.5 J/cm^2, and an oxygen partial pressure was 0.05 mTorr. The substrate temperature during TCO thin film deposition was maintained at 70 °C.

Dielectric Function of Ga:ZnO. The optical properties of Ga:ZnO films and the annealed films were characterized by spectroscopic ellipsometry (V-VASE, J.A. Woollam) in the spectral region from 350 to 2500 nm. The dielectric function of the films was retrieved by fitting a Drude + Lorentz oscillator model to the ellipsometry data. The following equation describes the Drude + Lorentz oscillator model where the second term comes from the Drude model and the third term represents the Lorentz oscillator. The retrieved model parameters are listed in Table 1.

$$\varepsilon(\omega) = \varepsilon_\infty - \frac{\omega_p^2}{\omega(\omega + i\Gamma_p)} + \frac{f_l\omega_l^2}{\omega_l^2 - \omega^2 - i\omega\Gamma_l}$$

Table 1. Drude + Lorentz Model Parameters for TCOs

	ε_∞	ω_p (eV)	Γ_p (eV)	f_l	ω_l (eV)	Γ_l (eV)
Ga:ZnO (as-deposited)	2.475	2.06	0.089	1.054	5.560	0.001
Ga:ZnO (annealed at 300 °C)	2.471	1.903	0.089	0.986	5.533	0.001
Ga:ZnO (annealed at 450 °C)	2.468	1.735	0.090	0.937	5.530	0.001

AUTHOR INFORMATION

Corresponding Author

*E-mail: aeb@purdue.edu.

Notes

The authors declare no competing financial interest.

ACKNOWLEDGMENTS

The Purdue team is supported by the U.S. Army Research Office Grant 63133-PH (W911NF-13-1-0226) "Flat Photonics with Metasurfaces" and the Air Force Office of Scientific Research MURI Grant FA9550-14-1-0389 "Active Metasurfaces for Advanced Wavefront Engineering and Waveguiding". A.A. and Y.Z. were supported by the Welch foundation with Grant No. F-1802 and AFOSR with Grant No. FA9550-13-1-0204.

REFERENCES

(1) Kildishev, A. V.; Boltasseva, A.; Shalaev, V. M. Planar Photonics with Metasurfaces. *Science* **2013**, *339*, 1232009.

(2) Ni, X.; Emani, N. K.; Kildishev, A. V.; Boltasseva, A.; Shalaev, V. M. Broadband Light Bending with Plasmonic Nanoantennas. *Science* **2012**, *335*, 427−427.

(3) Yu, N.; Capasso, F. Flat Optics with Designer Metasurfaces. *Nat. Mater.* **2014**, *13*, 139−150.

(4) Huang, L.; Chen, X.; Mühlenbernd, H.; Zhang, H.; Chen, S.; Bai, B.; Tan, Q.; Jin, G.; Cheah, K.-W.; Qiu, C.-W. Three-Dimensional Optical Holography Using a Plasmonic Metasurface. *Nat. Commun.* **2013**, *4*, 2808.

(5) Montelongo, Y.; Tenorio-Pearl, J. O.; Williams, C.; Zhang, S.; Milne, W. I.; Wilkinson, T. D. Plasmonic Nanoparticle Scattering for Color Holograms. *Proc. Natl. Acad. Sci. U. S. A.* **2014**, *111*, 12679−12683.

(6) Ni, X.; Kildishev, A. V.; Shalaev, V. M. Metasurface Holograms for Visible Light. *Nat. Commun.* **2013**, *4*, 2807.

(7) Chen, W. T.; Yang, K.-Y.; Wang, C.-M.; Huang, Y.-W.; Sun, G.; Chiang, I.-D.; Liao, C. Y.; Hsu, W.-L.; Lin, H. T.; Sun, S.; et al. High-Efficiency Broadband Meta-Hologram with Polarization-Controlled Dual Images. *Nano Lett.* **2014**, *14*, 225−230.

(8) Chen, X.; Huang, L.; Mühlenbernd, H.; Li, G.; Bai, B.; Tan, Q.; Jin, G.; Qiu, C.-W.; Zhang, S.; Zentgraf, T. Dual-Polarity Plasmonic Metalens for Visible Light. *Nat. Commun.* **2012**, *3*, 1198.

(9) Pors, A.; Nielsen, M. G.; Eriksen, R. L.; Bozhevolnyi, S. I. Broadband Focusing Flat Mirrors Based on Plasmonic Gradient Metasurfaces. *Nano Lett.* **2013**, *13*, 829−834.

(10) Aieta, F.; Genevet, P.; Kats, M. A.; Yu, N.; Blanchard, R.; Gaburro, Z.; Capasso, F. Aberration-Free Ultrathin Flat Lenses and Axicons at Telecom Wavelengths Based on Plasmonic Metasurfaces. *Nano Lett.* **2012**, *12*, 4932−4936.

(11) Kim, M.; Wong, A. M.; Eleftheriades, G. V. Optical Huygens' Metasurfaces with Independent Control of the Magnitude and Phase of the Local Reflection Coefficients. *Phys. Rev. X* **2014**, *4*, 041042.

(12) Pors, A.; Albrektsen, O.; Radko, I. P.; Bozhevolnyi, S. I. Gap Plasmon-Based Metasurfaces for Total Control of Reflected Light. *Sci. Rep.* **2013**, *3*, 02155.

(13) Yu, N.; Aieta, F.; Genevet, P.; Kats, M. A.; Gaburro, Z.; Capasso, F. A Broadband, Background-Free Quarter-Wave Plate Based on Plasmonic Metasurfaces. *Nano Lett.* **2012**, *12*, 6328−6333.

(14) Zhao, Y.; Alù, A. Manipulating Light Polarization with Ultrathin Plasmonic Metasurfaces. *Phys. Rev. B: Condens. Matter Mater. Phys.* **2011**, *84*, 205428.

(15) Roberts, A.; Lin, L. Plasmonic Quarter-Wave Plate. *Opt. Lett.* **2012**, *37*, 1820−1822.

(16) Khoo, E. H.; Li, E. P.; Crozier, K. B. Plasmonic Wave Plate Based on Subwavelength Nanoslits. *Opt. Lett.* **2011**, *36*, 2498−2500.

(17) Drezet, A.; Genet, C.; Ebbesen, T. W. Miniature Plasmonic Wave Plates. *Phys. Rev. Lett.* **2008**, *101*, 043902.

(18) Gansel, J. K.; Thiel, M.; Rill, M. S.; Decker, M.; Bade, K.; Saile, V.; von Freymann, G.; Linden, S.; Wegener, M. Gold Helix Photonic Metamaterial as Broadband Circular Polarizer. *Science* **2009**, *325*, 1513−1515.

(19) Shaltout, A.; Liu, J.; Kildishev, A.; Shalaev, V. Photonic Spin Hall Effect in Gap−Plasmon Metasurfaces for On-Chip Chiroptical Spectroscopy. *Optica* **2015**, *2*, 860−863.

(20) Zhao, Y.; Alù, A. Tailoring the Dispersion of Plasmonic Nanorods to Realize Broadband Optical Meta-Waveplates. *Nano Lett.* **2013**, *13*, 1086−1091.

(21) Pors, A.; Nielsen, M. G.; Della Valle, G.; Willatzen, M.; Albrektsen, O.; Bozhevolnyi, S. I. Plasmonic Metamaterial Wave Retarders in Reflection by Orthogonally Oriented Detuned Electrical Dipoles. *Opt. Lett.* **2011**, *36*, 1626−1628.

(22) Jiang, S.-C.; Xiong, X.; Hu, Y.-S.; Hu, Y.-H.; Ma, G.-B.; Peng, R.-W.; Sun, C.; Wang, M. Controlling the Polarization State of Light with a Dispersion-Free Metastructure. *Phys. Rev. X* **2014**, *4*, 021026.

(23) Grady, N. K.; Heyes, J. E.; Chowdhury, D. R.; Zeng, Y.; Reiten, M. T.; Azad, A. K.; Taylor, A. J.; Dalvit, D. A.; Chen, H.-T. Terahertz

DOI: 10.1021/acsnano.6b03937
ACS Nano 2016, 10, 9326−9333

Metamaterials for Linear Polarization Conversion and Anomalous Refraction. *Science* **2013**, *340*, 1304−1307.
(24) Yang, Y.; Wang, W.; Moitra, P.; Kravchenko, I. I.; Briggs, D. P.; Valentine, J. Dielectric Meta-Reflectarray for Broadband Linear Polarization Conversion and Optical Vortex Generation. *Nano Lett.* **2014**, *14*, 1394−1399.
(25) Naik, G. V.; Shalaev, V. M.; Boltasseva, A. Alternative Plasmonic Materials: Beyond Gold and Silver. *Adv. Mater.* **2013**, *25*, 3264−3294.
(26) Boltasseva, A.; Atwater, H. A. Low-Loss Plasmonic Metamaterials. *Science* **2011**, *331*, 290−291.
(27) Li, S.-Q.; Guo, P.; Buchholz, D. B.; Zhou, W.; Hua, Y.; Odom, T. W.; Ketterson, J.; Ocola, L. E.; Sakoda, K.; Chang, R. P. Plasmonic−Photonic Mode Coupling in Indium-Tin-Oxide Nanorod Arrays. *ACS Photonics* **2014**, *1*, 163−172.
(28) Kim, J.; Naik, G. V.; Gavrilenko, A. V.; Dondapati, K.; Gavrilenko, V. I.; Prokes, S.; Glembocki, O. J.; Shalaev, V. M.; Boltasseva, A. Optical Properties of Gallium-Doped Zinc Oxide—A Low-Loss Plasmonic Material: First-Principles Theory and Experiment. *Phys. Rev. X* **2013**, *3*, 041037.
(29) Gordon, T. R.; Paik, T.; Klein, D. R.; Naik, G. V.; Caglayan, H.; Boltasseva, A.; Murray, C. B. Shape-Dependent Plasmonic Response and Directed Self-Assembly in a New Semiconductor Building Block, Indium-Doped Cadmium Oxide (ICO). *Nano Lett.* **2013**, *13*, 2857−2863.
(30) Naik, G. V.; Kim, J.; Boltasseva, A. Oxides and Nitrides as Alternative Plasmonic Materials in the Optical Range. *Opt. Mater. Express* **2011**, *1*, 1090−1099.
(31) Gregory, S. A.; Wang, Y.; de Groot, C. H.; Muskens, O. L. Extreme Subwavelength Metal Oxide Direct and Complementary Metamaterials. *ACS Photonics* **2015**, *2*, 606−614.
(32) Li, S. Q.; Guo, P.; Zhang, L.; Zhou, W.; Odom, T. W.; Seideman, T.; Ketterson, J. B.; Chang, R. P. Infrared Plasmonics with Indium−Tin-Oxide Nanorod Arrays. *ACS Nano* **2011**, *5*, 9161−9170.
(33) Abb, M.; Wang, Y.; Papasimakis, N.; de Groot, C.; Muskens, O. L. Surface-Enhanced Infrared Spectroscopy Using Metal Oxide Plasmonic Antenna Arrays. *Nano Lett.* **2014**, *14*, 346−352.
(34) Kim, J.; Dutta, A.; Memarzadeh, B.; Kildishev, A. V.; Mosallaei, H.; Boltasseva, A. Zinc Oxide Based Plasmonic Multilayer Resonator: Localized and Gap Surface Plasmon in the Infrared. *ACS Photonics* **2015**, *2*, 1224−1230.
(35) Kim, J.; Naik, G. V.; Emani, N. K.; Guler, U.; Boltasseva, A. Plasmonic Resonances in Nanostructured Transparent Conducting Oxide Films. *IEEE J. Sel. Top. Quantum Electron.* **2013**, *19*, 4601907−4601907.
(36) Wang, Y.; Capretti, A.; Dal Negro, L. Wide Tuning of the Optical and Structural Properties of Alternative Plasmonic Materials. *Opt. Mater. Express* **2015**, *5*, 2415−2430.
(37) Alu, A.; Engheta, N. *Optical Wave Interaction with Two-Dimensional Arrays of Plasmonic Nanoparticles*; Cambridge University Press: Cambridge, UK, 2011; pp 58−93.
(38) Silveirinha, M. G. Nonlocal Homogenization Model for a Periodic Array of ϵ-Negative Rods. *Phys. Rev. E* **2006**, *73*, 046612.
(39) Kim, J.; Dutta, A.; Naik, G. V.; Giles, A. J.; Bezares, F. J.; Ellis, C. T.; Tischler, J. G.; Mahmoud, A. M.; Caglayan, H.; Glembocki, O. J.; Kildishev, A. V.; Caldwell, J. D.; Boltasseva, A.; Engheta, N. Role of Epsilon-Near-Zero Substrates in the Optical Response of Plasmonic Antennas. *Optica* **2016**, *3*, 339−346.
(40) Kabashin, A.; Evans, P.; Pastkovsky, S.; Hendren, W.; Wurtz, G.; Atkinson, R.; Pollard, R.; Podolskiy, V.; Zayats, A. Plasmonic Nanorod Metamaterials for Biosensing. *Nat. Mater.* **2009**, *8*, 867−871.
(41) Yang, C.; Shen, W.; Zhang, Y.; Peng, H.; Zhang, X.; Liu, X. Design and Simulation of Omnidirectional Reflective Color Filters Based on Metal-Dielectric-Metal Structure. *Opt. Express* **2014**, *22*, 11384−11391.

DOI: 10.1021/acsnano.6b03937
ACS Nano 2016, 10, 9326−9333